Magnetization Transfer in Lamellar Liquid Crystals

Dariya I. Malyarenko,[1] Ellen M. Zimmermann,[2] Jeremy Adler,[3] and Scott D. Swanson[1]*

Purpose: This study examines the relationship between quantitative magnetization transfer (qMT) parameters and the molecular composition of a model lamellar liquid crystal (LLC) system composed of 1-decyl alcohol (decanol), sodium dodecyl sulfate (SDS), and water.

Methods: Samples were made within a stable lamellar mesophase to provide different ratios of total semisolid protons (SDS + decanol) to water protons. Data were collected as a function of radiofrequency power, frequency offset, and temperature. qMT parameters were estimated by fitting a standard model to the data. Fitting results of four different semisolid line shapes were compared.

Results: A super-Lorentzian line shape for the semisolid component provided the best fit. The estimated amount of semisolids was proportional to the ratio of decanol-to-water protons. Other qMT parameters exhibited nonlinear dependence on sample composition. Magnetization transfer ratio (MTR) was a linear function of the semisolid fraction over a limited range of decanol concentration.

Conclusion: In LLC samples, MT between semisolid and water originates from intramolecular nOe among decanol aliphatic chain protons followed by proton exchange between decanol hydroxyl and water. Exchange kinetics is influenced by SDS, although SDS protons do not participate in MT. These studies provide clinically relevant range of semisolid fraction proportional to detected MTR. **Magn Reson Med 72:1427–1434, 2014. © 2013 Wiley Periodicals, Inc.**

Key words: magnetization transfer; MRI; MT phantom; super-Lorentzian

INTRODUCTION

Magnetization transfer (MT) MRI takes advantage of interactions between water and the semisolid components of tissue to indirectly image the semisolid fraction by means of the detected water protons. Application of an MT preparation pulse increases image contrast for tissue in regions where water is efficiently coupled to the semisolid component. The ratio of the difference image to the image obtained without MT preparation, termed magnetization transfer ratio (MTR), is used in clinical research to increase lesion conspicuity without exogenous contrast agents (1–6). Several clinical MT studies have been performed primarily in neurological applications in disease such as multiple sclerosis (2,4,7,8), Alzheimer's disease (AD) (5), and focal cortical dysplasia in children (6). Other studies indicate that MTR is correlated with tissue fibrosis and could be used to distinguish between inflammation and fibrosis in Crohn's disease (3,9).

When the MT experiment is performed as a function of radiofrequency (RF) power and frequency offset of the preparation pulse, quantitative magnetization transfer (qMT) parameters can be extracted by fitting to an appropriate model of semisolid component line shape, relaxation, and exchange properties (10,11). In clinical research, qMT has been used to measure the amount of semisolid component, which correlates with myelin content of white matter (12–14). A decrease of semisolid magnetization in the hippocampus was observed in qMT studies of patients with AD (15–17).

While progress has been made to bring MT into clinical use, an optimal MR sequence for selective tissue contrast does not yet exist. Standard MT imaging is influenced by a complicated ratio of relaxation and cross-relaxation parameters that reduces tissue specificity and hinders diagnostic utility (18,19). qMT pulse sequences could alleviate some of these problems, but requires long acquisition times and significant post processing. Furthermore, a detailed picture of the physics of the molecular level processes underlying MT remains cloudy. A comprehensive theoretical development and model validation has been hampered in part by the lack of an appropriate model system. The desired model system should both mimic tissue characteristics and allow manipulation of components to produce predictable alterations in MT properties reflected in the fitted model parameters.

Current MT theory relies on the hypothesis that the semisolid proton fraction in tissue can be described by a single, homogeneously broadened resonance of arbitrary shape (10,20). Different theoretical semisolid model line shapes were found appropriate for empiric description of MT depending on specific molecular properties of the semisolid-pool. Initial development of MT theory used a Gaussian function to model the line shape of the semisolid component (10,20). Based on work of Wennerstrom (21) and Bloom et al. (22), a super-Lorentzian (SL) line shape was found to be more appropriate for MT data collected from white matter and gray matter (23). A homogeneously broadened SL line shape has subsequently become part of the standard MT model for neurological studies using qMT (23,24) and has been used successfully to fit direct detection of the myelin line by NMR (25).

[1]Department of Radiology, University of Michigan, Ann Arbor, Michigan, USA.

[2]Department of Internal Medicine - Gastroenterology, University of Michigan, Ann Arbor, Michigan, USA.

[3]Department of Pediatrics and Communicable Diseases, University of Michigan, Ann Arbor, Michigan, USA.

Grant sponsor: National Institutes of Health; Grant numbers: NIH T32 EB005172, NIH R01 DK073992.

*Correspondence to: Scott D. Swanson, Ph.D., Department of Radiology, University of Michigan, 1301 Catherine Street, 3208A Medical Science I, Ann Arbor, MI 48109. E-mail: sswanson@umich.edu

Additional supporting information may be found in the online version of this article.

Received 11 July 2013; revised 18 September 2013; accepted 15 October 2013

DOI 10.1002/mrm.25034

Published online 20 November 2013 in Wiley Online Library (wileyonlinelibrary.com).

Most model MT systems studied to date have used either cross-linked bovine serum albumin (BSA) (26) or polysaccharides (10). While these materials may provide an appropriate MT model for proteins in muscle tissue or polysaccharides in hyaline cartilage, they do not adequately represent the MT physics occurring in the phospholipid membranes of white matter and gray matter (2,7,8). A more appropriate model for neural tissue would be a lipid membrane system. These systems have been extensively studied by NMR, particularly deuterium NMR (27,28), yet only a few MT studies have been reported. Ceckler et al surveyed different macromolecular systems including phospholipid membranes for evidence of MT (29). Fralix et al identified cholesterol as a key component to induce MT in lipid systems (30). In one of the more complete studies, Kucharczyk et al examined MT in synthetic white matter lipids (31) and concluded that galacto-cerebroside content (in addition to cholesterol) and pH have the strongest effect on MT. None of the studies to date provided a full survey of qMT parameters and their relation to the chemical and physical properties of the lipid membranes.

Mixtures of surfactants, water, and alcohols form well-characterized systems (32–34) that mimic many properties of biological membranes. We have found that these lyotropic, lamellar liquid crystals (LLCs, as surrogate biological membranes) generate MT between the water and the aliphatic (semisolid) components and allow numerous molecular permutations to help disentangle qMT properties. LLCs possess many desired characteristics for MT studies, such as: a large MT-effect, simple sample preparation, stability (during long storage), and a quantitative relation between components and qMT-model parameters. This work focuses on how the molar ratio of semisolid protons (decanol and sodium dodecyl sulfate [SDS]) to water protons influences qMT parameters, such as the estimated semisolid fraction, M_0^b, cross-relaxation rate R_t, and transverse relaxation time of semisolid, T_{2b}, in LLCs composed of SDS, decanol, and water. Different compositions are explored to understand chemical–physical background of MT with the purpose to ultimately use this knowledge in connection to clinical MTR-studies as related to in vivo effects (1–6).

METHODS

LLC Samples

A series of samples were constructed with deionized-distilled water, SDS (99%, molecular biology grade, Sigma-Aldrich, St. Louis, MO), and 1-decyl alcohol (decanol) (>98%, Sigma-Aldrich, St. Louis, MO) to satisfy three conditions. First, the relative amounts of ingredients were chosen so that the samples were all in a stable, lamellar mesophase of the ternary phase diagram for this system (34). Second, the mole fractions of components were selected to create samples with two different weight fraction of water (C_W = grams of water/total sample weight). Four samples were made with $C_W = 45\%$ and five samples with $C_W = 65\%$. Third, within each water weight fraction, the mole fraction of decanol to total lipid protons was varied from 0.41 to 0.62. This allowed study of samples with similar water content but differing semisolid components. The vials were sealed and then vortexed, centrifuged, heated to 55°C (to improve sample miscibility), cooled to room temperature, and aged over 72hr to ensure sample uniformity. These steps ensured organization of the components into the lamellar phase (34). A representative diagram of the lamellar mesophase (34) at $C_W = 45\%$ is shown in Figure 1.

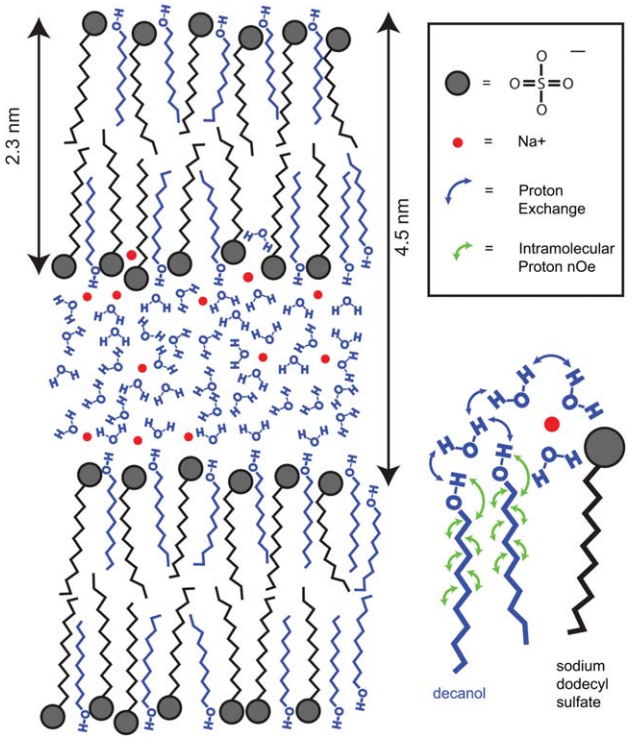

FIG. 1. Conceptual diagram of the LLC phase formed by hydrophobic bilayers of SDS (black) and decanol (blue) chains that encapsulate polar water layer (blue) and sodium ions (red). The distances are given for water content of $C_W = 45\%$ as measured by small angle X-ray scattering (SAXS) experiments Ref. (34). Blue color indicates LLC components (decanol and water) participating in MT. The insert on the right focuses on a subset of the polar / nonpolar interface to reflect the MT mechanism between decanol and water protons consistent with our experimental findings, i.e., proceeding by means of hydroxyl proton exchange (blue arrows) and aliphatic proton nOe (green arrows). Terminal chain segments of decanol are excluded from MT due to probable large amplitude motions.

The final composition of the prepared samples is described in terms of the molar fractions of water protons, X_W, decanol protons, X_D, and SDS protons, X_{SDS}. Samples were made in following ranges: $X_W = 0.44$–0.67, $X_D = 0.14$–0.34, and $X_{SDS} = 0.13$–0.31. A sample mixed with D_2O was prepared at a single concentration. All samples were stored at room temperature. (Details of sample compositions and results are presented in Supp. Table S1, which is available online).

NMR Data Acquisition

To collect data for model fitting and qMT parameter estimation, continuous wave (CW) RF irradiation (10 s) was

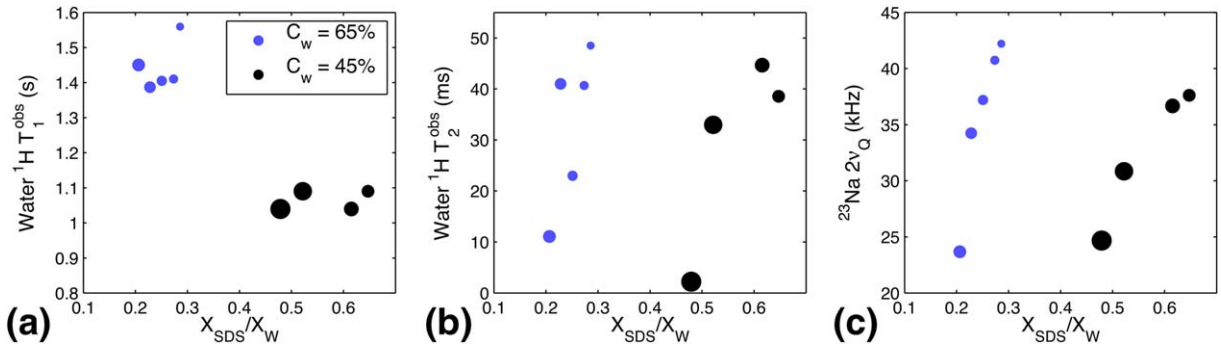

FIG. 2. Experimentally observed parameters are plotted as a function of the ratio of mole fraction of SDS protons, X_{SDS}, to mole fraction of water protons, X_W, for T_1^{obs} (**a**), T_2^{obs} (**b**), and ^{23}Na quadrupole splitting $2\nu_Q$ (**c**). The symbol diameter is proportional to mole fraction of decanol protons, X_D. The exponential fit errors for relaxation times [omitted in (a) and (b)] were within the symbol boundaries. The measurement error for $2\nu_Q$ was ±300 Hz. The samples with high versus low water content (C_W = 65% versus C_W = 45%) are indicated by different colors, as shown in Figure 2 (a).

applied at four power levels and nineteen off-resonance frequencies at 2T. The water proton T_1 and T_2 (T_1^{obs} and T_2^{obs}) were measured in separate experiments using standard inversion-recovery (IR) and Carr-Purcell-Meiboom-Gill (CPMG) pulse sequences. To study the effect of SDS counterion on qMT parameters, ^{23}Na spectra were acquired for all samples at 22°C, using spectral width (sw) = 100kHz, pulse width (pw) = 4μs, and repetition time (TR) = 0.2s. The measured frequency difference between the $|3/2\rangle \rightarrow |1/2\rangle$ and $|-1/2\rangle \rightarrow |-3/2\rangle$ transitions (=$2\nu_Q$) was analyzed. To directly observe both the water proton and semisolid proton resonances, a ^{1}H spectrum (sw = 100 kHz, pw = 4μs, TR = 5s) of a sample (C_W = 65%) prepared with D_2O was obtained. In addition to MT studies at room temperature after preparation, three samples were studied at 40°C, and two samples (with 45% and 65% water content) were rerun at room temperature after prolonged storage (over 6 months).

MT Fit Models and Parameters

A two-compartment exchange model was used to fit the observed MT-curves and extract physical parameters (10). A Matlab toolbox was developed for nonlinear least squares fit that included options of Lorentzian (L) and Gaussian (G) line shapes (10), as well as mixed super-Lorentzian (SL) (23,35) and correlation-time (KCT, Kubo-Tomita) (36) models for the semisolid component. Model fidelity-metrics was provided by mean-squared-error (MSE) obtained by means of the estimate of variance of the error term for nonlinear least squares "nlinfit" function (Matlab 7, Mathworks, Natick, MA). Fit parameter errors were estimated as the square-root of diagonal elements of the covariance matrix provided by the "nlinfit".

The best fit values of MT parameters, obtained with SL model, M_0^b, R_t, T_{2b}, T_{2a}, and R_a, were estimated and analyzed across all studied LLC samples (Supp. Table S1). The fit model included frequency offset for the semisolid component resonance to account for the observed ^{1}H chemical shift of aliphatic protons contributing to MT. The frequency offset was set to 320 Hz relative to water for all reported fits. The errors for R_t and T_{2b} parameters were calculated directly from the fit, while the confidence interval for M_0^b, T_{2a}, and R_a were obtained by standard error propagation using both fit errors for parameter combinations from "nlinfit" and the T_1^{obs} errors.

RESULTS

Figures 2a and 2b show observed spin relaxation times for water, T_1^{obs} and T_2^{obs}, as a function of the ratio of SDS protons to water protons (X_{SDS}/X_W). Figure 2c presents the measured dependence of ^{23}Na quadrupole splitting, $2\nu_Q$, on X_{SDS}/X_W. To aid visualization of the effect of decanol on the measured NMR parameters, the marker diameters in Figure 2 are proportional to the mole fraction of decanol protons, X_D. In addition, data from samples with higher water content are drawn with blue markers. The average measurement errors were within 1.5% (less than marker size) and are omitted from the plots. As evident from Figure 2a, T_1^{obs} exhibits a step-like change with water content, from an average of 1.45s for C_W = 65% to 1.05s for C_W = 45%, and is otherwise nominally independent of the composition of the semisolid fraction.

Within each C_W family, both T_{2obs} and $2\nu_Q$ (Figs. 2b,c) are generally increasing with increasing SDS proton fraction (decreasing decanol content). The observed $2\nu_Q$ between 22 and 43 kHz reflected the strength of electric field gradient in the vicinity of ^{23}Na nucleus at the semisolid surface (37). The average ratio of $2\nu_Q$ measured for samples with high versus low semisolid content (C_W = 45% versus C_W = 65%) at fixed ratio of SDS-to-decanol content was close to one (37.6/42.2 kHz and 24.7/23.7 kHz), while $2\nu_Q$ ratio for lower versus higher relative SDS content at fixed water weight fraction was ~0.6 (23.7/42.2 kHz and 24.7/37.6 kHz). These results report on increasing local charge density near sodium counterions on lamellae surface (37) mainly due to increasing relative SDS amount in semisolid phase (independent of C_W).

Figure 3a illustrates ^{1}H-NMR results for the sample prepared in D_2O. The ~320 Hz chemical shift is observed between residual protonated water and the aliphatic protons of semisolid component. The broad spectral line shape is indicative of complex (non-Lorentzian) relaxation of the semisolid fraction. Also shown in Figure 3a is a simulated super-Lorentzian (SL) line shape with T_{2b} = 20 μs. Comparison of the experimental and simulated lines suggest that the prevailing fraction of the

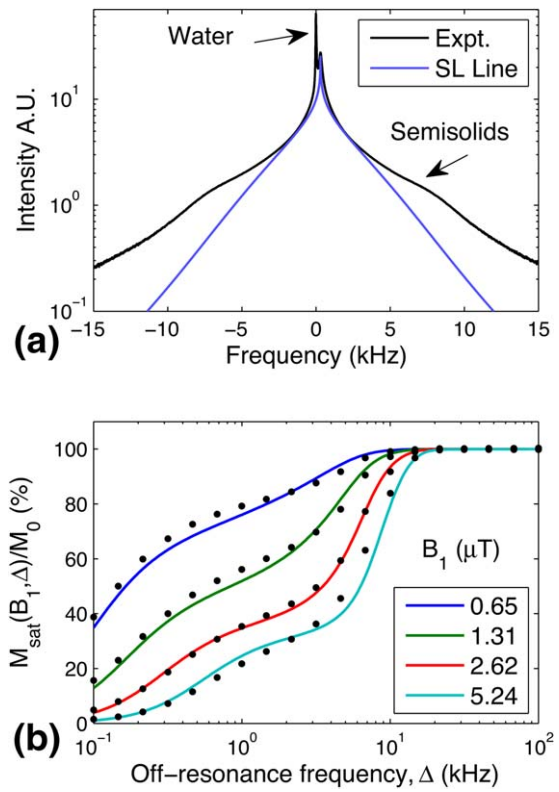

FIG. 3. **a:** ^{1}H-NMR spectrum of LLC made with D_2O (black line) is plotted on a log-intensity scale along with the best fit super-Lorentzian line shape (blue line) for the semisolid component participating in MT. The semisolid component fit is offset by 320Hz to account for the chemical shift of the decanol aliphatic protons at 2T. **b:** An example of fitting qMT model (lines) based on offset super-Lorentzian to collected data (dots) at different power levels of applied MT pulse (see legend for color-codes). These data are for the LLC sample with $C_W = 65\%$ and $X_D/X_{SDS} = 0.22/0.13$.

semisolid component expected to participate in MT can be adequately modeled by an SL line shifted from the water resonance by ~320 Hz. The shoulder-like features at ±8 kHz likely indicate residual dipole–dipole interactions among aliphatic protons.

Figure 3b provides an example of fitting MT model to collected data with super-Lorentzian semisolid line shape offset of 320 Hz for the LLC sample. The MSE error of the super-Lorentzian fit was 2.7%. Inclusion of the frequency offset reduced the fit MSE by 0.2% for all samples (average MSE = 3%). For comparison, the fit using Lorentzian (L) and Gaussian (G) models produced much higher MSE of 20% and 5.5%, respectively. For majority of samples, MSE with L and G model was approximately 5- and 2-times higher than that of super-Lorentzian fit (MSE~3%). Correlation time model (KCT) produced MSE comparable to (~0.5% lower than) that with SL fit, but included extra fit parameters. The main effect of 320 Hz frequency offset included in the SL MT-model was in approximately 20–30% increase of fit M_0^b and proportional decrease in R_t values compared with zero-offset. The observed increase of fit M_0^b is consistent with inclusion of higher fraction of semisolid protons in the description of MT process. Other qMT parameters were not significantly affected by the offset: the observed < 5% change was within their corresponding confidence intervals of 10–15%.

Table 1 lists fit parameters obtained using different line shape models for the semisolid component for two representative samples (with 65% and 45% water fraction). The SL model line shape best captures mixed characteristics of compact G- and smooth L-curves (Supp. Fig. S1), but has a singularity on resonance. The KCT model preserves general characteristics of Gaussian line shape, providing smooth coverage over a broader frequency range. The fit values for M_0^b listed in Table 1 are the closest to the decanol proton fraction in the sample for the SL model. Apparently, this model accounts for the largest fraction of semisolid component in LLC samples compared with other models. SL $T_{2b} \sim 20$ μs, on the other hand, is the shortest among the models and independent of semisolid fraction. For the mobile fraction, the estimate of fit parameters (R_a and T_{2a}) for super-Lorentzian is consistent with Lorentzian results, which is physically appropriate model for the mobile component. Both G and KCT models underestimate T_{2a} and likely overestimate T_{2b} due to their compact line shapes (Table 1, Supp. Fig. S1). A Lorentzian model results in the largest fit error (MSE) for MT experiments, which indicates its inadequacy for semisolid fraction description in the LLC samples. Other than for Lorentzian, exchange rate fit parameter values, R_t, are consistent between the models within uncertainty limits. Overall, SL model provides most physically relevant picture of both semisolid and mobile components and, presumably, their interaction. KCT model introduces additional fit parameter, τ_c, that describes a correlation time for the semisolid component

Table 1
Fit Parameters for Different MT Models: Super-Lorentzian (SL), Lorentzian (L), Gaussian (G), Kubo Correlation-Time (KCT)

C_w	Model	R_a (s^{-1})	R_t (s^{-1})	M_0^b	T_{2a} (ms)	T_{2b}/τ_c (μs)	MSE (%)
65%	SL	0.62 ± 0.01	6.7 ± 0.7	0.22 ± 0.04	13.1 ± 0.8	21.7 ± 0.4	2.4
	L	0.65 ± 0.02	14.7 ± 4.3	0.14 ± 0.07	14 ± 2	111 ± 14	17.7
	G	0.64 ± 0.01	7.8 ± 0.9	0.16 ± 0.03	10.3 ± 0.5	44.3 ± 0.6	3.9
	KCT	0.643 ± 0.008	8.6 ± 0.7	0.15 ± 0.02	11.3 ± 0.5	38.8 ± 0.6 33 ± 5(τ_c)	1.6
45%	SL	0.87 ± 0.02	10 ± 1	0.52 ± 0.1	27 ± 2	21.4 ± 0.3	2.7
	L	0.88 ± 0.03	21 ± 7	0.33 ± 0.2	28 ± 6	103 ± 9	25
	G	0.88 ± 0.02	10.2 ± 1.5	0.41 ± 0.1	18 ± 1	45.3 ± 0.7	6
	KCT	0.88 ± 0.02	12 ± 1	0.39 ± 0.07	21 ± 1	39 ± 0.6 25 ± 3(τ_c)	2.3

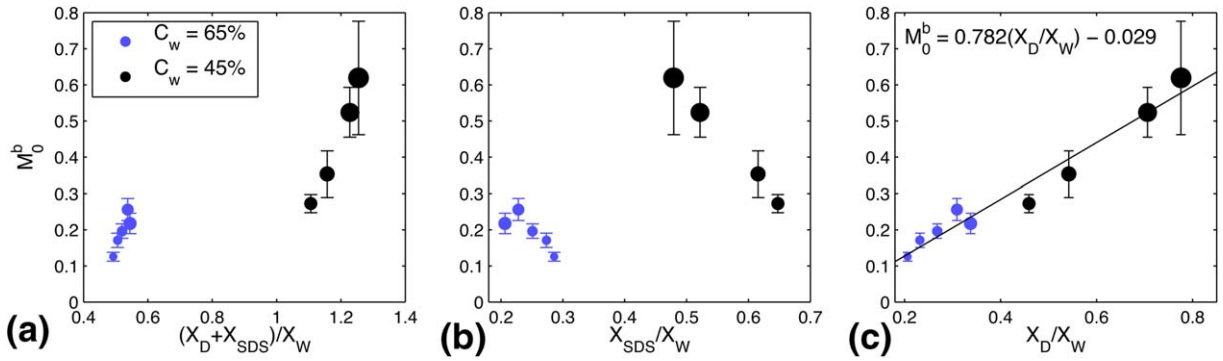

FIG. 4. M_0^b plotted as a function of molar ratio of the total semisolid protons, X_D/X_{SDS}, to water protons, X_W, in (**a**); molar ratio of SDS to water protons in (**b**); and of the molar ratio of decanol protons to water protons in (**c**). The data symbol diameter in (a–c) is proportional to mole fraction of the decanol protons, X_D. The samples with high versus low water content ($C_W = 65\%$ versus $C_W = 45\%$) are indicated by different color, as shown in (a). The linear fit parameters for (c) are listed in the line-fit equation. The error bars represent one standard deviation of nonlinear least squares fit for qMT-model.

protons. Its value decreases from 33 ± 5 to 25 ± 3 μs when water content increases from 45% to 65%.

MT theory (10) predicts that M_0^b should be proportional to the molar ratio of semisolid protons to water protons. Figure 4a plots M_0^b as a function this ratio, $(X_D + X_{SDS})/X_W$, and clearly shows that this proportionality is not observed for LLC samples. For each weight percent, C_W, there is an increase of M_0^b with increasing semisolid proton fraction, but there is also a large discontinuity between the individual C_W sets. Figure 4b shows the estimated semisolid proton fraction as a function of the ratio of SDS protons to water protons (X_{SDS}/X_W) and reveals that M_0^b decreases as X_{SDS}/X_W increases within each of the C_W groups. Figure 4c confirms that M_0^b is proportional to the molar ratio of decanol protons to water protons, X_D/X_W. The slope of the linear fit (0.78) likely reflects the fraction of decanol protons participating in MT.

Figure 5 illustrates dependence of other qMT-fit parameters on X_{SDS}/X_W. Similar to Figures 2 and 4, the diameter of the markers in Figure 5 are proportional to X_D and the marker color reflects water content. R_a (Fig. 5a) increases as water content decreases, and is otherwise independent of SDS or decanol fraction, similar to observed longitudinal relaxation (Fig. 2a). Linear regression between $R_1^{obs} = 1/T_1^{obs}$ and R_a ($r^2 = 0.994$) yields an intercept of 0.095 and a slope of 0.93. R_t (Fig. 5b) marginally increases with increased SDS content or conversely decreases with increased decanol content; however, the dependence is not monotonic. T_{2b} is relatively constant (Fig. 5c, 22±2 μs) for all nine samples. T_{2a} exhibits a general, but weakly correlated, increases as a function of SDS protons (Fig. 5d) and decreases as decanol increases. T_{2a} behavior is qualitatively similar to that of R_t (Fig. 5b) and T_2^{obs} (Fig. 2b).

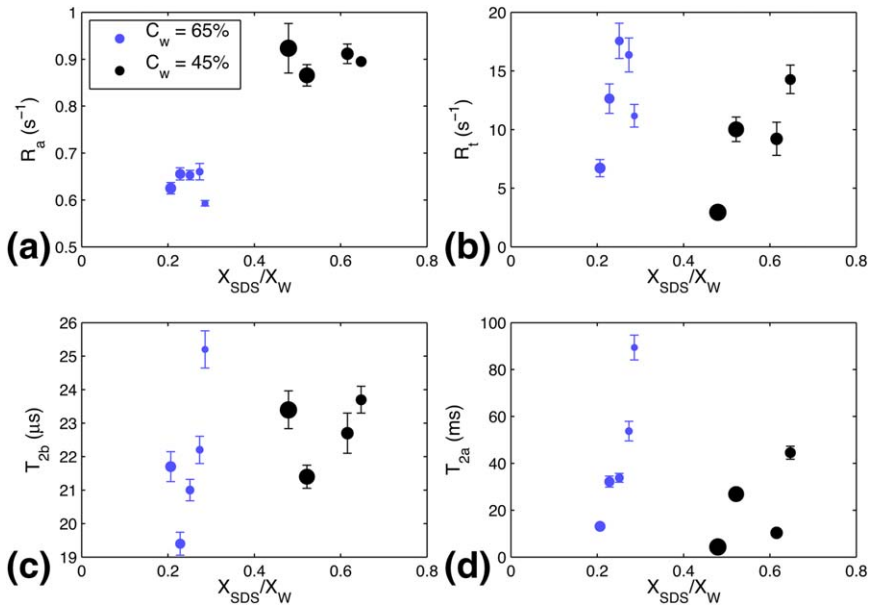

FIG. 5. qMT-fit parameters plotted as a function of the molar ratio of SDS-to-water protons, X_{SDS}/X_W: (**a**) R_a; (**b**) R_t; (**c**) T_{2b} and (**d**) T_{2a}. The data symbol diameter in (a–d) is proportional to mole fraction of the decanol protons, X_D. The samples with high versus low water content ($C_W = 65\%$ versus $C_W = 45\%$) are indicated by different color, as shown in Figure 5a. The error bars represent one standard deviation of nonlinear least squares fit for qMT-model.

Table 2
Temperature Dependence of MT-Fit Parameters with Super-Lorentzian Line Shape Model for Three Representative LLC Samples

C_w	T ± 1, °C	R_a (s^{-1})	R_t (s^{-1})	M_0^b	T_{2b} (μs)	T_{2a} (ms)
65%	22	0.66 ± 0.01	16.4 ± 1.4	0.158 ± 0.025	21.8 ± 0.4	82.6 ± 6
	40	0.4 ± 0.01	9.5 ± 0.9	0.161 ± 0.03	28.9 ± 0.5	89.6 ± 8
65%	22	0.62 ± 0.01	6.7 ± 0.7	0.22 ± 0.04	21.7 ± 0.4	13.1 ± 0.8
	40	0.39 ± 0.02	4.9 ± 0.6	0.26 ± 0.06	27.0 ± 0.4	15.5 ± 1.4
45%	22	1.15 ± 0.06	8.9 ± 1.3	0.6 ± 0.17	21.3 ± 0.4	5 ± 0.5
	40	0.67 ± 0.06	8.8 ± 1.2	0.63 ± 0.24	27.5 ± 0.5	11 ± 2

Temperature dependence of MT-fit parameters is summarized in Table 2 for three representative LLC samples. A decrease of approximately 40% in R_a is observed with increasing temperature. For samples with C_W =65% (lower decanol + SDS), a proportional decrease is also observed for R_t, but the effect is negligible for a sample with high semisolid-fraction. Marginal increase is observed for absolute M_0^b (~2–4%) along with the noticeable increase in T_{2a} and T_{2b}. Prolonged storage (data not shown) of a sample with higher semisolid fraction (C_W = 45%) resulted in higher R_a and M_0^b, as well as lower R_t, but had almost no effect (except for higher T_{2a}) on MT-parameters of a sample with lower semisolid component.

Figure 6 uses the values of the estimated room temperature qMT parameters to calculate MTR assuming an RF amplitude of 5 μT and off-resonance frequencies of 2, 4.6, and 10 kHz to plot MTR as a function of X_D/X_W (proportional to M_0^b, as illustrated in Fig. 4c). The relationship is linear for $X_D/X_W < 0.3$ and plateaus at higher semisolid fraction. This general behavior is independent of frequency offset (different symbols) or power (not shown).

DISCUSSION

The results of this study elucidate the chemical and physical origins of quantitative MT parameters in LLC model systems. This understanding provides insight into development of viable qMT phantoms, optimization of MT acquisition in clinical environment, and appropriate interpretation of in vivo MT results (1–8). Although the presented findings are specific to LLC samples, the uncovered involvement of basic molecular interactions in MT processes is applicable to diverse model systems (10,26,29–31). As MRI evolves to become a tool for molecular imaging, understanding the detailed molecular origin of MT contrast and qMT parameters will be important to aid in a more specific description of disease progression and treatment.

The presented analysis of ^{1}H NMR line shapes supported application of the two-component exchange model (with a single line shape for semisolid fraction) to account for magnetization transfer in LLC samples. However, the reported fit results should be interpreted as the average qMT-parameters of the multicomponent system due to different motion and chemical shifts of the aliphatic protons of the decanol chain participating in MT. These protons resonate between 3.25 and 3.92 ppm upfield from the water resonance (measured between 280 and 335 Hz at 2T), and line shapes and relaxation properties are expected to vary. Nevertheless, adequate description of MT processes for different LLC sample compositions is achieved with minimal number of fit parameters using single super-Lorentzian lineshape model for a semisolid component.

Detected linear dependence of estimated M_0^b on the ratio of decanol protons to water protons indicates that in LLC chemical system, decanol protons are the primary species participating in MT with water. The hydroxyl groups of decanol provide exchangeable protons that serve as an MT vehicle for spin diffusion from protons down the decanol chain (Fig. 1). The higher mobility of remote chain segments (consistent with line shape and relaxation analysis) prevents their full participation in MT, which is reflected in lower correlation (0.78 < 1) of linear fit for M_0^b. Higher consistency of MT-parameters after long storage observed for higher water content (65%) sample likely indicates better stability of the corresponding LLC phase, which may be useful for MT-phantom design. Observed ~35% increase in M_0^b-fit after long storage of lower water content (C_W = 45%) sample can be indicative of tendency to expel water due to high content of decanol + SDS hydrophobic chains reordering with time.

Our measurements confirm that the observed water relaxation time, T_1^{obs}, is sensitive to the water content of the sample but not the molecular constituents of the semisolid phase. A similar pattern is detected for the estimated parameter, R_a, the relaxation rate of water protons in absence of cross-relaxation. The change in T_1^{obs} reflects the change in water layer thickness (from 5.1 to

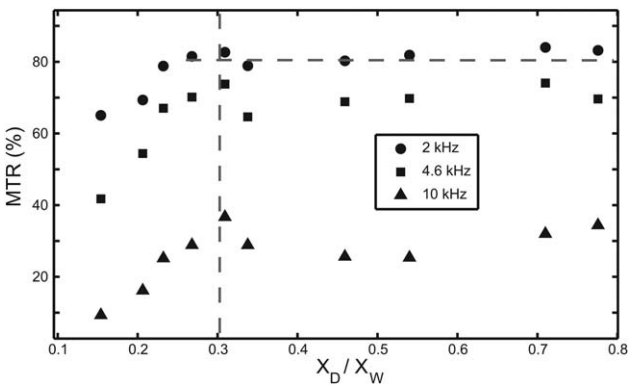

FIG. 6. Percent MTR at 5 μT RF MT-pulse for three frequency offsets (see legend for symbol assignment) as a function of the molar ratio of decanol-to-water protons (directly proportional to M_0^b in Fig. 4). The vertical dashed line indicates the range of semisolid fractions (participating in MT) that can be quantitatively inferred from direct MTR measurements. The horizontal dashed line illustrates the lack of detectible variation in MTR for decanol-to-water fractions above 0.3.

2.2 nm) (34). Decreased water layer thickness creates an increase in the surface-to-volume ratio and slows the average water rotational correlation by increased interaction with the surface, leading to an increased water relaxation rate. Therefore, as evident from linear regression slope between T_1^{obs} and R_a, approximately 93% of the observed water proton relaxation can be explained by the motion of water inside the lamellae (Fig. 1). After accounting for hydrodynamic effects, approximately 7% of the observed T_1 remains generated by cross-relaxation with the semisolid components. Noticeable (~40%) decrease in R_a observed with temperature increasing from 20 to 40°C (Table 2) is consistent with a decreased water rotational correlation time at higher temperatures.

In contrast, the decrease in T_2^{obs} with increasing decanol content observed (at fixed C_W) is due to population-weighted exchange of water protons (long T_{2a}) with short T_{2b} decanol protons. This result is consistent with previous studies for similar lamellar systems (38). The observed similarity of trends for T_2^{obs} and $2\nu_Q$ implicates correlation between local charge density around ^{23}Na nucleus (37) and decanol-water exchange processes. This correlation can be explained by enhanced water coordination near lamellae surface for samples with higher SDS content that facilitates exchange with proximal decanol protons (Fig. 1). This explanation is also consistent with observed behavior of both estimated MT cross-relaxation rate, R_t, and the estimated water proton T_{2a}.

A marginal decrease in R_t observed with increasing decanol content, as well as increase in M_0^b and decrease in R_t observed with increasing temperature for samples with 65% water fraction (Table 2), can be explained by competition between MT-exchange and energy preferred water coordination in sodium hydration sphere (Fig. 1). This is not an Arrhenius activation process, because exchange rate decreases with increasing temperature (Table 2) and exhibits concentration dependence on LLC components. We hypothesize that this feature is due to thermal motion competing with hydration energy (especially at higher water content). This motion frees more sodium *aqua* ions to participate in exchange with decanol hydroxyl protons thereby slightly increasing apparent M_0^b with lower R_t.

This hypothesis is supported by our observation of changes in local environment for sodium hydration shell as a function of LLC components as well as temperature dependence of MT parameters (Table 2). Detected high (>20 kHz) absolute values as well as substantial increase (~40%) in sodium quadrupole splitting with increasing relative SDS amount (~50%) is consistent with increasing local charge density around counterions condensed on lamellae surface (37). For samples with high water fraction, which have intrinsically lower repulsion between lamellae (34), this increase can be related to increasing surface area of the sodium hydration shell. At higher temperatures, enhanced molecular motion within lamellae and mobile phase, as evident from longer T_{2b} and T_{2a} (Table 2), would destabilize the hydration shell, consequently decreasing exchange rate between semisolid and mobile components. Longer T_{2a} observed with increasing temperature (Table 2) is consistent with higher mobility of water when thermal energy disrupts hydrogen bonding around sodium. These results may be generally relevant for understanding the indirect influence of "MT-neutral" component (like SDS and sodium ions) on MT parameters in multi-component system (Fig. 1). Thus, model LLC systems may serve as proxies for describing effect of ions on MT kinetics in biological membranes.

In the studied samples, T_{2b}, indicative of the rigidity of the immobilized component, does not depend on sample composition. Estimated T_{2b} is significantly longer (2- to 3-times) than the 10–15 μs typically observed in vivo (39). Unlike the shorter chain lengths in the LLC model membranes (decanol is a ten carbon chain molecule and SDS is a 12 carbon chain molecule) biological membranes are composed primarily of phospholipids with chains of 16 to 18 carbon atoms. In addition, cholesterol and imbedded membrane proteins will increase membrane rigidity. T_{2b} of model membranes can be shortened by using longer chain alcohols or fatty acids. T_{2b} increases from approximately 22 μs at 22°C to approximately 28 μs at 40°C (Table 2) indicating significant increased motion within semisolid part of the liquid crystal with increased temperature. This increased motion will reduce the negative intermolecular nOe (between decanol and SDS) and quench spin diffusion (Fig. 1).

Studies of qMT in vivo find M_0^b to be 0.14 in white matter and 0.06 in gray matter (24). Using known proton content in brain of lipids, proteins, and water, one can calculate a theoretical semisolid mole fraction of 0.25 in white matter and 0.14 in gray matter. The mismatch between MT-estimated and theoretical values is similar to our finding in model systems. Our experimental studies show that not all aliphatic protons participate in MT in the model LLC membranes. Implicit involvement of cholesterol and galacto-cerebrosides in MT processes have been demonstrated (30,31), but a quantitative relationship between M_0^b and lipid protons has not yet been established. Therefore, it is still unclear what specific molecules of white and gray matter are measured in qMT experiments in vivo.

Our results suggest that percent MT (MTR) measurements that are usually performed on clinical scanners would have a limited dynamic range (<0.3) where the changes in semisolid component can be "detected" directly from experimental data with reliable accuracy. The relative changes in MTR for semisolid fraction above 0.3 are within 5%, and could be masked by experimental measurement error. This baseline sensitivity needs to be taken into account when the MTR contrast is used as clinical biomarker (2–6). As shown above, M_0^b obtained from the qMT model estimate is clearly proportional to the semisolid fraction over the full range of concentrations. However, obtaining the fit M_0^b requires long data acquisition at several frequency offsets and MT-pulse power levels, which may not be clinically viable. MTR plot for LLC in Figure 6 suggests limited range of linearity with growing semisolid fraction (<0.3). As is shown by above estimates, this range is applicable for clinical measurements.

CONCLUSIONS

LLC samples provide a convenient model to study the molecular properties of MT representative of in vivo

systems and allow a more complete and consistent molecular picture of MT. In the studied LLC systems composed of SDS, decanol, and water, detected MT was found to originate by exchange of hydroxyl decanol protons with water and to percolate by intramolecular nOe from aliphatic protons. The most consistent description of MT-process both for semisolid and mobile components was obtained using super-Lorentzian line shape model. Estimated M_0^b represents a subset of the semisolid fraction, because significant motion of molecular segments partially quenches NOE and spin diffusion from remote protons toward the end of the aliphatic chain. Water proton relaxation, R_a, is directly determined by interlamellae membrane spacing. The rate of exchange between semisolid and mobile component reports on available pool of exchangeable protons controlled by water coordination around ionic species. The region of linear dependence between MTR and semisolid-like fraction (<0.3) is relevant for clinical studies. The study of MT in this model system allows finding the range of semisolid fraction were MTR contrast could be used directly for clinical monitoring of changes in biological membranes.

REFERENCES

1. Henkelman RM, Stanisz GJ, Graham SJ. Magnetization transfer in MRI: a review. NMR Biomed 2001;14:57–64.
2. Filippi M, Absinta M, Rocca MA. Future MRI tools in multiple sclerosis. J Neurol Sci 2013;331:14–18.
3. Adler J, Swanson SD, Schmiedlin-Ren P, Higgins PDR, Golembeski CP, Polydorides AD, McKenna BJ, Hussain HK, Verrot TM, Zimmermann EM. Magnetization transfer helps detect intestinal fibrosis in an animal model of Crohn disease. Radiology 2011;259:127–135.
4. Bodini B, Cercignani M, Toosy A, Stefano ND, Miller DH, Thompson AJ, Ciccarelli O. A novel approach with "skeletonised MTR" measures tract-specific microstructural changes in early primary-progressive MS. Hum Brain Mapp 2014;35:723–733.
5. Mascalchi M, Ginestroni A, Bessi V, Toschi N, Padiglioni S, Ciulli S, Tessa C, Giannelli M, Bracco L, Diciotti S. Regional analysis of the magnetization transfer ratio of the brain in mild Alzheimer disease and amnestic mild cognitive impairment. Am J Neuroradiol 2013;34: 2098–2104.
6. Kadom N, Trofimova A, Vezina GL. Utility of magnetization transfer T1 imaging in children with seizures. AJNR Am J Neuroradiol 2013; 34:895–898.
7. Grossman RI. Application of magnetization transfer imaging to multiple sclerosis. Neurology 1999;53:S8–S11.
8. Filippi M, Campi A, Dousset V, Baratti C, Martinelli V, Canal N, Scotti G, Comi G. A magnetization transfer imaging study of normal-appearing white matter in multiple sclerosis. Neurology 1995;45:478–482.
9. Adler J, Rahal K, Swanson SD, et al. Anti-tumor necrosis factor α prevents bowel fibrosis assessed by messenger RNA, histology, and magnetization transfer MRI in rats with Crohn's disease. Inflamm Bowel Dis 2013;19:683–690.
10. Henkelman RM, Huang XM, Xiang QS, Stanisz GJ, Swanson SD, Bronskill MJ. Quantitative interpretation of magnetization transfer. Magn Reson Med 1993;29:759–766.
11. Sled JG, Pike GB. Quantitative imaging of magnetization transfer exchange and relaxation properties in vivo using MRI. Magn Reson Med 2001;46:923–931.
12. Tozer D, Ramani A, Barker GJ, Davies GR, Miller DH, Tofts PS. Quantitative magnetization transfer mapping of bound protons in multiple sclerosis. Magn Reson Med 2003;50:83–91.
13. Schmierer K, Tozer DJ, Scaravilli F, Altmann DR, Barker GJ, Tofts PS, Miller DH. Quantitative magnetization transfer imaging in postmortem multiple sclerosis brain. J Magn Reson Imaging 2007;26:41–51.
14. Levesque I, Sled JG, Narayanan S, Santos AC, Brass SD, Francis SJ, Arnold DL, Pike GB. The role of edema and demyelination in chronic T1 black holes: a quantitative magnetization transfer study. J Magn Reson Imaging 2005;21:103–110.
15. Hanyu H, Shimizu S, Tanaka Y, Kanetaka H, Iwamoto T, Abe K. Differences in magnetization transfer ratios of the hippocampus between dementia with Lewy bodies and Alzheimer's disease. Neurosci Lett 2005;380:166–169.
16. Kiefer C, Brockhaus L, Cattapan-Ludewig K, Ballinari P, Burren Y, Schroth G, Wiest R. Multi-parametric classification of Alzheimer's disease and mild cognitive impairment: the impact of quantitative magnetization transfer MR imaging. Neuroimage 2009;48:657–667.
17. Giulietti G, Bozzali M, Figura V, Spano B, Perri R, Marra C, Lacidogna G, Giubilei F, Caltagirone C, Cercignani M. Quantitative magnetization transfer provides information complementary to grey matter atrophy in Alzheimer's disease brains. Neuroimage 2012;59:1114–1122.
18. Rosenkrantz AB, Storey P, Gilet AG, Niver BE, Babb JS, Hajdu CH, Lee VS. Magnetization transfer contrast-prepared MR imaging of the liver: inability to distinguish healthy from cirrhotic liver. Radiology 2011;262:136–143.
19. Homayoon N, Ropele S, Hofer E, Schwingenschuh P, Seiler S, Schmidt R. Microstructural tissue damage in normal appearing brain tissue accumulates with Framingham Stroke Risk Profile Score: magnetization transfer imaging results of the Austrian Stroke Prevention Study. Clin Neurol Neurosurg 2013;115:1317–1321.
20. Swanson SD. Transient and steady-state effects of indirect RF saturation in heterogeneous systems. In Proceedings of the 11th Annual Meeting of SMRM, Berlin, Germany, 1992.
21. Wennerstrom H. Proton nuclear magnetic-resonance lineshapes in lamellar liquid-crystals. Chem Phys Lett 1973;18:41–44.
22. Bloom M, Burnell EE, Roeder S, Valic MI. Nuclear magnetic-resonance line-shapes in lyotropic liquid-crystals and related systems. J Chem Phys 1977;66:3012–3020.
23. Morrison C, Stanisz G, Henkelman RM. Modeling magnetization-transfer for biological-like systems using a semisolid pool with a super-Lorentzian lineshape and dipolar reservoir. J Magn Reson B 1995;108:103–113.
24. Stanisz GJ, Odrobina EE, Pun J, Escaravage M, Graham SJ, Bronskill MJ, Henkelman RM. T1, T2 relaxation and magnetization transfer in tissue at 3T. Magn Reson Med 2005;54:507–512.
25. Wilhelm MJ, Ong HH, Wehrli SL, Li C, Tsai P-H, Hackney DB, Wehrli FW. Direct magnetic resonance detection of myelin and prospects for quantitative imaging of myelin density. Proc Natl Acad Sci U S A 2012;109:9605–9610.
26. Grad J, Bryant RG. Nuclear Magnetic Cross-Relaxation Spectroscopy. J Magn Reson 1990;90:1–8.
27. Seelig J. Deuterium magnetic resonance: theory and application to lipid membranes. Q Rev Biophys 1977;10:353–418.
28. Brown MF, Ribeiro AA, Williams GD. New view of lipid bilayer dynamics from H-2 and C-13 NMR relaxation-time measurements. Proc Natl Acad Sci U S A 1983;80:4325–4329.
29. Ceckler TL, Wolff SD, Yip V, Simon SA, Balaban RS. Dynamic and chemical factors affecting water proton relaxation by macromolecules. J Magn Reson 1992;98:637–645.
30. Fralix TA, Ceckler TL, Wolff SD, Simon SA, Balaban RS. Lipid bilayer and water proton magnetization transfer - effect of cholesterol. Magn Reson Med 1991;18:214–223.
31. Kucharczyk W, Macdonald PM, Stanisz GJ, Henkelman RM. Relaxivity and magnetization-transfer of white-matter lipids at MR-imaging - importance of cerebrosides and pH. Radiology 1994;192:521–529.
32. Quist PO, Halle B, Furo I. Nuclear-spin relaxation in a hexagonal lyotropic liquid-crystal. J Chem Physics 1991;95:6945–6961.
33. Halle B, Quist PO, Furo I. Microstructure and dynamics in lyotropic liquid-crystals - principles and applications of nuclear-spin relaxation. Liq Cryst 1993;14:227–263.
34. Berger K, Hiltrop K. Characterization of structural transitions in the SLS/decanol/water system. Colloid Polym Sci 1996;274:269–278.
35. Morrison C, Henkelman RM. A model for magnetization-transfer in tissues. Magn Reson Med 1995;33:475–482.
36. Kubo R, Tomita K. A General theory of magnetic resonance absorption. J Phys Soc Jpn 1954;9:888–919.
37. Wennerstrom H, Lindman B, Linblom G, Tiddy GJT. Ion condensations model and nuclear magnetic resonance studies of counterion binding in lyotropic liquid crystals. J Chem Soc Faraday Trans 1 1979;75:663–668.
38. Tiddy GJT. NMR relaxation times of the lamellar phases of the system sodium caprylate/decanol/water. J Chem Soc Faraday Trans 1 1972;68:369–380.
39. Sled JG, Levesque I, Santos AC, Francis SJ, Narayanan S, Brass SD, Arnold DL, Pike GB. Regional variations in normal brain shown by quantitative magnetization transfer imaging. Magn Reson Med 2004; 51:299–303.